LHCb 2000-065 RICH
September 4, 2000

Proposal for Multi-Anode Photo Multiplier Tubes as Photo Detectors for the LHCb RICH

F. Muheim[1], University of Edinburgh
on behalf of the MAPMT group[2]

Abstract

We propose to use Multianode Photo Multiplier Tubes (MAPMT) as the photosensitive device for the Ring Imaging Cherenkov (RICH) detector in the LHCb experiment. We demonstrate that MAPMT meet the specifications which are required to perform excellent particle identification of charged tracks over the full acceptance. A baseline design is presented. At the end of 1999 the MAPMT has been selected as backup choice for the photo detectors. We present the implication of this decision to the baseline design.

[1]Corresponding author. Email: F.Muheim@ed.ac.uk
[2]V. Gibson, S. Katvars, S. Wotton, University of Cambridge
E. Albrecht, CERN
R. Bernet, S. Eisenhardt, F. Muheim, S. Playfer, University of Edinburgh
S. Cuneo, A. Petrolini, M. Sannino, University of Genova
S. Easo, A. Halley, University of Glasgow
G. Barber, A. Duane, D. Price, B. Simmons, D. Websdale, Imperial College, London
M. Calvi, C. Matteuzzi, M. Paganoni, Universita degli Studi di Milano
J. Bibby, M. Charles, N. Harnew, J. Libby, J.Rademacker, N. Smale, S. Topp-Jorgensen, G.Wilkinson, University of Oxford
J. Baker, C. Densham, M. French, Rutherford Appleton Laboratory

1 Introduction

In this document we propose to use multianode photomultiplier tubes (MAPMT) as the photosensitive device for the Ring Imaging Cherenkov (RICH) detector in the LHCb experiment. The proposal consists of the following parts: In Section 1.1, the LHCb RICH detector layout and its main parameters are shortly summarised. A more detailed discussion is given in the Technical Proposal [1]. Additional information can be obtained from the LHCb RICH web page [2]. The MAPMTs and their characteristics are described in Section 2, followed by a summary of the R&D results in Section 3. The proposal of a baseline design is discussed in detail in Section 4. Additional documents which were prepared for the photo detector choice panel are appended.

1.1 LHCb RICH Detectors

The LHCb RICH detectors are shown schematically in Figure 1. The difference in scale of the two detectors should be noted. The RICH system consists of an upstream detector, RICH 1, with both a 5 cm thick silica aerogel and ∼95 cm length of C_4F_{10} gas radiator, and a downstream detector, RICH 2, with a ∼180 cm length of CF_4 gas radiator. The three radiators are required to cover the full LHCb momentum range. The angular acceptances extend between approximately 25–330 mrad (RICH 1) and 10–120 mrad (RICH 2). Although RICH 2 has a reduced acceptance, it catches a large fraction of the high momentum tracks, e.g. 90% of reconstructed pions from $B^0_d \to \pi^+\pi^-$ with $p > 70$ GeV/c which are beyond the limit for π–K separation in RICH 1. The pion thresholds are 0.6, 2.6, and 4.4 GeV/c for the aerogel (refractive index, n=1.03), C_4F_{10} (n= 1.0014) and CF_4 (n=1.0005) radiators, respectively. Kaon thresholds are 2.0, 9.3 and 15.6 GeV/c, respectively.

In both RICH detectors, the Cherenkov photons are focused by mirrors to planes of photo detectors positioned outside the spectrometer acceptance. To shorten the overall length of the RICH 2 detector, the image from the spherical mirror is reflected by a second flat mirror to the detector planes. Assuming an active-area fraction of 73%, approximately 340 k electronic channels are required in total (140 k for RICH 1 and 200 k for RICH 2).

For the Technical Proposal it was assumed that the quantum efficiency of the photocathode is 28 % at its maximum value. The expected numbers of detected photoelectrons are 15 and 55 from aerogel and C_4F_{10} gas, respectively, for a fully saturated track ($\beta = 1$) in the RICH 1 detector. In the RICH 2 detector, approximately 30 detected photoelectrons are expected.

Good Cherenkov angle measurement resolution is crucial in achieving the required π-K discrimination. The design measurement resolutions are ∼1.45 mrad, 1.10 mrad and 0.35 mrad for aerogel, C_4F_{10} and CF_4, respectively. In the gas radiators, the resolution is made from approximately equal contributions from photon emission point uncertainty, chromatic aberration and finite photo detector pixel size. For the aerogel radiator, chromatic aberration dominates.

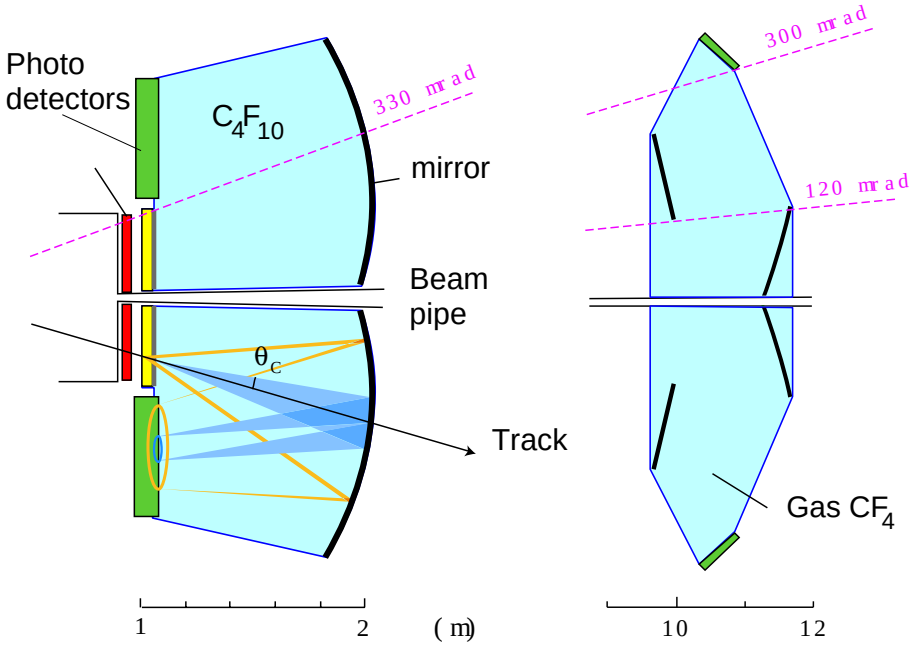

Figure 1: Layout of the upstream RICH 1 and downstream RICH 2 detectors, seen from above with the beam axis horizontal. The production of two rings in the photo detectors is illustrated for RICH 1.

Using a maximum likelihood analysis, reconstructed tracks of interest in simulated b-events are identified with efficiencies of $\sim 90\%$, and purities above 90%. A $3\,\sigma$ or larger separation of pions from kaons is achieved over the momentum range 1–100 GeV/c.

2 Multianode Photomultiplier Tubes

In this section we discuss the photo detector specifications and the MAPMT characteristics.

2.1 Photo Detector Specifications

The photo detectors for the LHCb RICH detectors must satisfy the following criteria :

- Single photons must be detected with high efficiency in both the visible and near ultra-violet. The ultra-violet sensitivity is advantageous to enhance the photon yield in the gaseous radiators, whereas visible light sensitivity is essential for the aerogel radiator (since Rayleigh scattering dominates in the ultra-violet).
- A large fraction of $\mathcal{O}(70\%)$ or more of the total area (2.9 m^2 for RICH 1 plus RICH 2) must be active.

- The spatial resolution necessitates a granularity of about 2.5 mm $\times$ 2.5 mm for each photon detection element.
- The cost per channel has to be low, $\mathcal{O}$(10 CHF).
- The readout must have low noise, and be fast enough for the 25 ns between LHC bunch crossings.
- The photo detectors must be able to cope (with iron shielding if necessary) with the fringe fields from the magnet, $\mathcal{O}$(1–100 Gauss), and survive radiation doses of a few krad/year.

2.2 Multianode Photomultiplier Characteristics

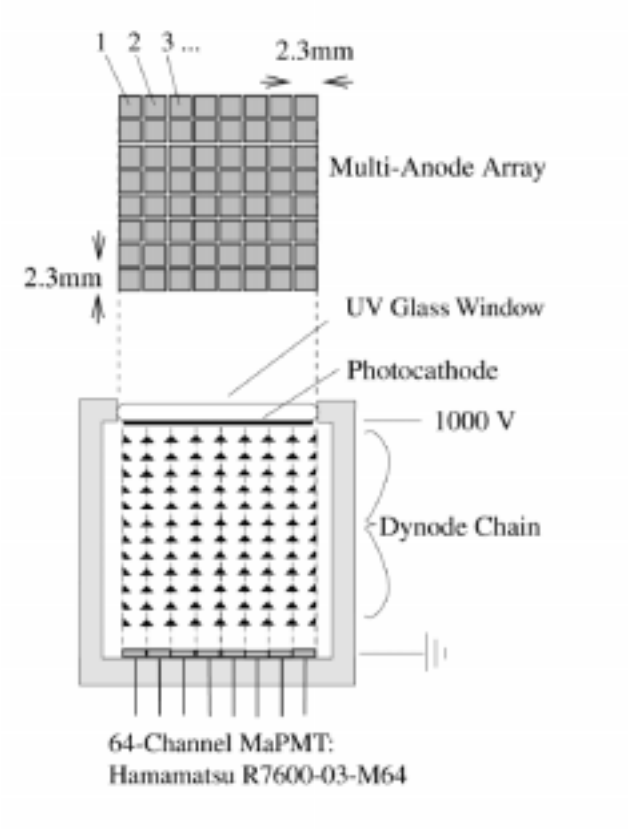

Figure 2: Sketch of a multianode photomultiplier tube.

A multianode photomultiplier tube consists of a square array of metal dynode chains incorporated into a single vacuum tube to amplify the photoelectrons. This pixelization provides good spatial resolution. A schematic of the detector technology is shown in Figure 2.

The proposed MAPMTs are currently commercially available, including some modifications provided by the manufacturer, Hamamatsu, during the last year to

better match our specifications. The MAPMT R7600-03-M64[3] has a 0.8 mm thick UV-glass window with the photocathode on the inside. The dynode structure is separated into 64 square pixels of 2.0 x 2.0 mm^2 area, separated by 0.3 mm gaps. The UV-glass window has a threshold of transmitted light at 200 nm. The photons are converted in a Bialkali photocathode. Figure 3 shows the quantum efficiency of the MAPMT which has a maximum of 22% at 380 nm. The specified gain is 3×10^5 at a voltage of 800 V. Nine MAPMTs have been purchased, preselected such that the average gain of the tubes varies not more than a factor of two.

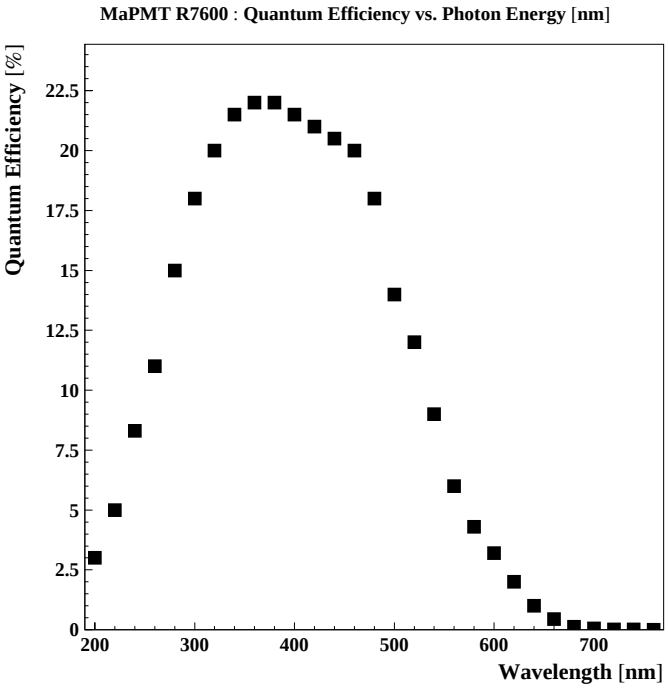

Figure 3: Quantum efficiency of the MAPMT R7600-03-M64 as a function of wavelength, measured by Hamamatsu.

The geometrical coverage of the MAPMT, i.e. the ratio of the sensitive photocathode area to the total tube area including the outer casing is only $\sim$ 48%. As proposed in reference [3] this fraction can be increased by placing a single lens with one refracting and one flat surface in front of each MAPMT (see Figure 4). In the thin lens approximation a single refracting surface with radius-of-curvature R has a focal length $f = \frac{R}{1-1/n}$ where n is the refractive index of the lens material. Figure 5 shows a schematic view of such a lens system in front of the close-packed photomultipliers. If the distance d of the refracting surface to the photocathode is chosen to be equal to R the demagnification factor is $(f-d)/f \approx 2/3$. Over the full aperture of the lens light at normal incidence with respect to the photodetector

[3]With respect to its predecessor, the R5900-00-M64, the borosilicate window is replaced by a UV-glass window which increases the integrated quantum efficiency by 50%. In addition, a flange of 1 mm size around the MAPMT is removed, thereby improving the packing fraction by 14%.

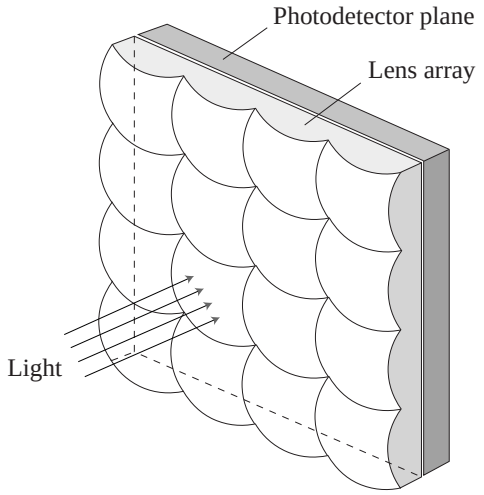

Figure 4: Isometric view of the lens array, mounted in front of the photo detector plane.

plane is focused onto the photocathode, thus restoring full geometrical acceptance. We can choose R but it must exceed half the diagonal width of the lens. The demagnification resulting from this lens configuration is illustrated in Figure 6. This demonstrates that the pin cushion distortion is small compared to the pixel size. The focusing is also quite independent of the angle of incidence of light. Nine quartz lenses, one for each MAPMT have been purchased. Their dimensions are square width of 26×26 mm^2, $R = 25$ mm and maximum height 24 mm.

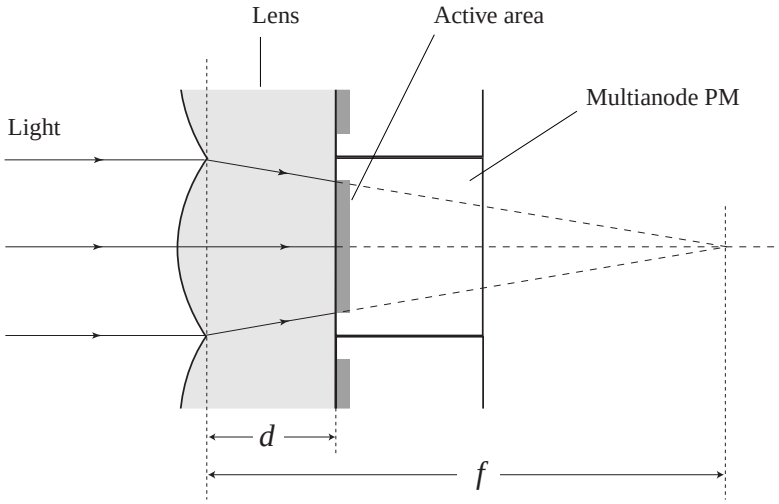

Figure 5: Schematic view of lens system, in front of the close-packed photomultipliers (side view). The focusing of normally incident light is illustrated. The full aperture of the lens is focused onto the sensitive area of the MAPMT.

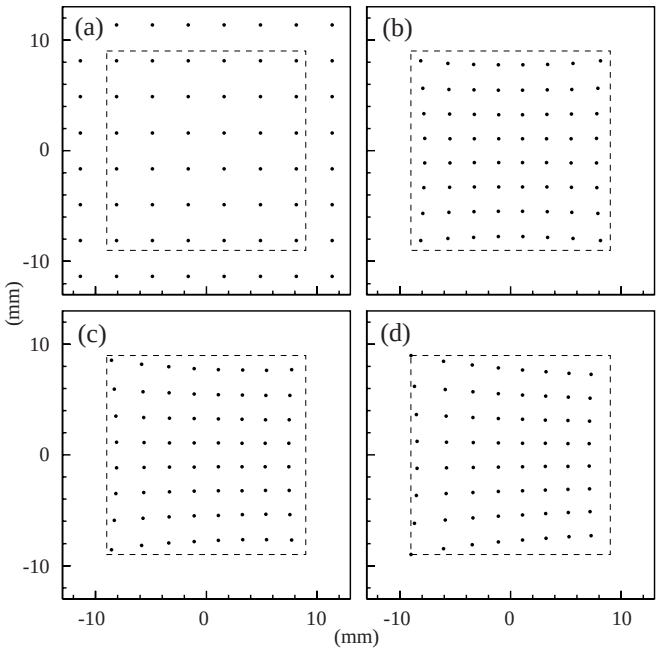

Figure 6: Impact points of a bundle of light rays incident on the entrance window of a multi-anode photomultiplier tube: (a) with no lens, (b-d) with a lens; (b) is for normally incident light, (c) and (d) are for an angle of incidence of 200 mrad and 400 mrad in the horizontal plane, respectively. The lens has been shifted with respect to the tube, accordingly. The solid (dashed) line indicates the the total (sensitive) area of the tube.

3 R & D Results

In this section we summarise the results from the MAPMT R&D effort that has been carried out. Most emphasis is given to recent measurements of 9 modified MAPMTs (R7600) delivered in May 1999 and their subsequent test using fast LHC speed (40 MHz) electronics. An update of these results with much more details can be found in the draft of the MAPMT test beam paper [4]. Earlier measurements can be found in References [5, 6, 7, 8].

3.1 LED Light Scans

A Hamamatsu MAPMT (R5900) has been tested on a light-scanning facility [6]. The MAPMT performs largely to the manufacturers specification; the gain variation and uniformity are typically within 20%. A study of the gap between the channels shows that the actual pixel size as defined by the 50% efficiency points of a pixel is 2.1 mm. This is a little larger than the 2.0 mm dynode opening stated by Hamamatsu.

Recently, the MAPMT R7600 has also been measured with the fast read-out (APVm, see Section 3.3). A signal spectrum is plotted in Figure 7. From these data, a ratio of the average signal position over the pedestal width (noise) of 40 is obtained. When requiring that a photo-electron signal is at least 5 noise σ above the pedestal position, this corresponds to a signal loss of 9 %. Comparing the width of the single photon peak with its position yields a lower limit of 3.7 for the gain at the first dynode. This corresponds to a probability of 2.5% or less for no multiplication occurring at the first dynode. Thus the total signal loss is 11.5%.

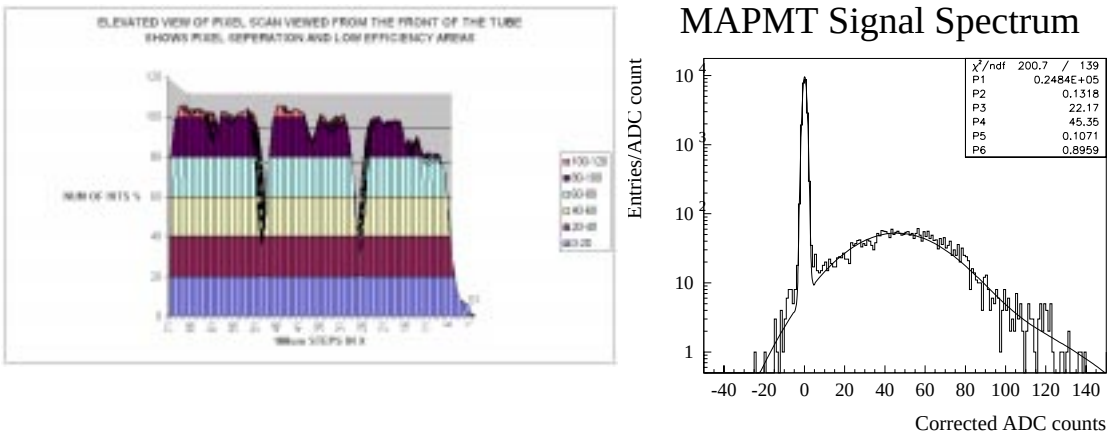

Figure 7: Left: Results of scanning with single photons across a 64-channel MAPMT.
Right: Single photon spectrum of a MAPMT pixel measured with the fast read-out (APVm) using a LED light source.

3.2 Testbeam with a Single MAPMT

The performance of a RICH 2 prototype detector, equipped with a MAPMT (R5900), has been studied with a charged particle beam at CERN during 1998. Using CAMAC front-end electronics, the signal loss for a 5 σ threshold cut has been estimated to be 8.5 %. The Cherenkov angle resolution, shown in Figure 8, is measured as 0.27 mrad, in good agreement with the expectation from the Monte Carlo simulation. The dominant contribution is due to the pixel size.

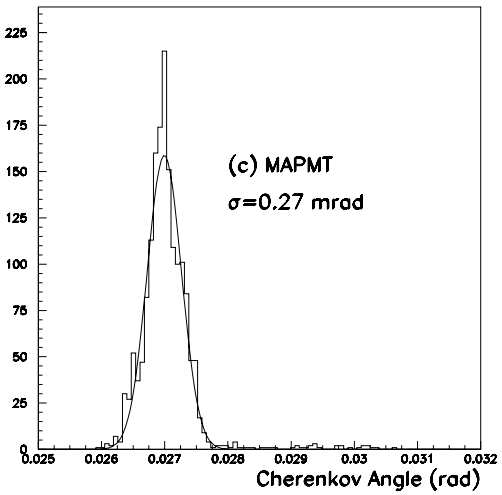

Figure 8: Cherenkov angle distribution for the MAPMT with CF_4 as radiator gas.

Recently the MAPMT R7600 has been mounted onto a RICH 1 prototype detector and exposed to charged particle beams. Using the CAMAC front-end electronics, data have been taken in different configurations, ie. with and without a quartz lens, 24 mm thick and with a radius of curvature of 25 mm, placed in front of the tube. With air at a pressure of 49 mbar as radiator the ring from the Cherenkov photons is focused onto the sensitive area of a single tube whereas at 960 mbar pressure only a partial ring can be observed. Figure 9 shows the Cherenkov rings for the low pressure measurements with and without a quartz lens placed in front of the tube. The effect of the lens is clearly visible. The measured yields of photo electrons for the different combinations and the corresponding expectations from a simulation are listed in Table 1. The total error on the these yields is estimated to be about 5%. The measurements are in good agreement with the expectations. From the low pressure runs where, up to reflection losses at the lens surfaces, the same number of photo electrons should be observed with and without the lens, it can be seen with little systematic uncertainty that the quartz lens works as expected. A second MAPMT has also been studied and the same yield of photo electrons as with the first tube was obtained.

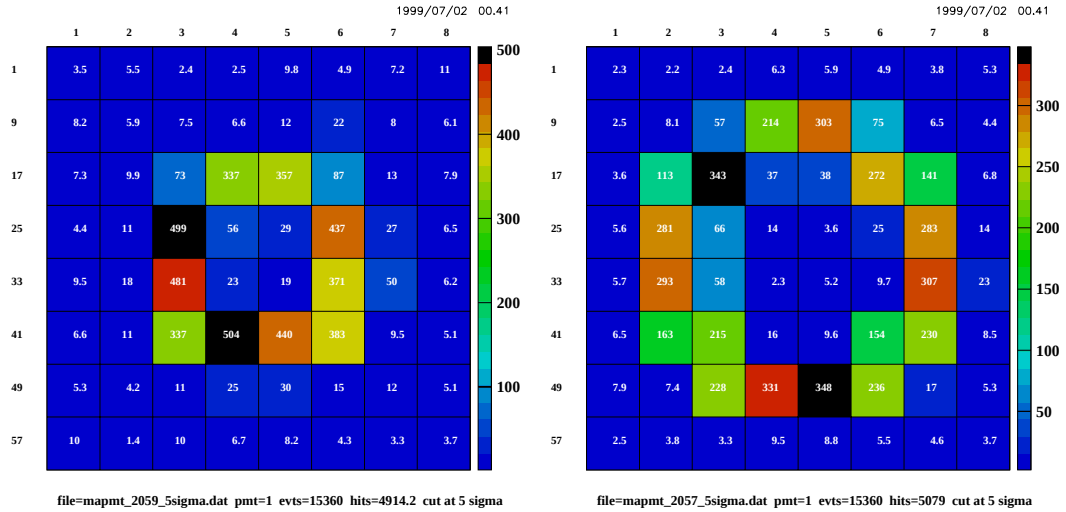

Figure 9: Cherenkov ring from air radiator at 49 mbar, measured with a single MAPMT. For the left (right) picture a (no) quartz lens has been place in front of the tube.

Pressure [mbar]	Lens	Data	Monte Carlo
49	No	0.32	0.32
49	Yes	0.30	0.29
960	No	0.93	0.89
960	Yes	1.14	1.16

Table 1: Comparison of data and Monte Carlo for the number of photo electrons measured with a single MAPMT.

3.3 MAPMT Cluster Tests at LHC Speed

During the summer of 1999 the performance of the MAPMT (R7600) has been studied with charged particle beams at CERN. The 9 MAPMTs have been mounted in a 3×3 array onto the full scale RICH 1 prototype detector, as shown in Figure 10. The vessel was filled with gaseous CF_4 at a pressure of 700 mbar, giving an expected Cherenkov angle of 26 mrad for highly relativistic particles. Measurements were taken with a 120 GeV/c π^- beam at intensities of typically a few 10^4 particles per spill of the CERN SPS cycle.

The primary goals of the MAPMT tests were as follows :

- To demonstrate that Cherenkov light can be detected over the full area of closely packed MAPMTs by means of quartz lenses focusing the light onto the sensitive area of the device.
- To demonstrate that MAPMTs can be read out at LHC speed, ie at 40 MHz.

The quartz lenses were mounted on the front faces of the the MAPMTs. The

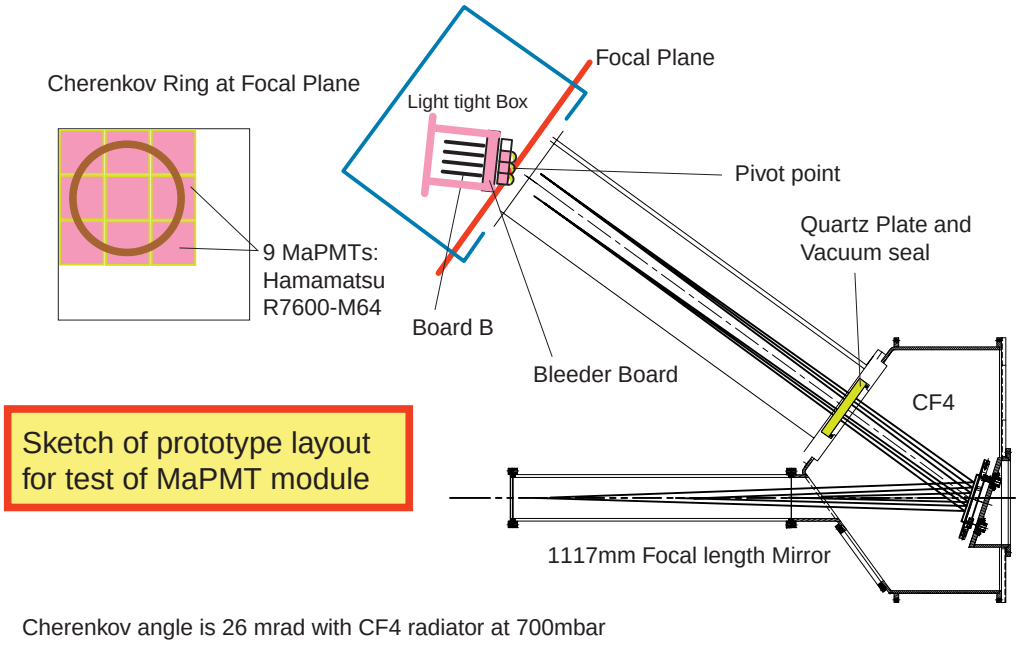

Figure 10: The MAPMT test beam setup.

APVm chip was chosen to study the LHC speed readout. Each 128-channel APVm sampled the signals of two MAPMTs. The chips were mounted on a carrier board together with a ceramic to attenuate the photomultiplier signals. Kapton cables were used to connect the anode pins of the HV "bleeder board" to the carrier boards.

This 40 MHz readout chain was employed successfully during a week of test beam running. About one million events were recorded under different conditions, eg: HV scan, with and without lenses, varying the angle of the MAPMT cluster with respect to the incoming photon direction. Figure 11 displays the integrated signals of a run of 6 k events, taken with lenses in front of the MAPMTs, the photocathodes at -1000 V and normal angle of incidence. The Cherenkov ring is clearly visible.

A cross-talk due to the electronics chain, in neighbouring channels in the APV sample and inputs, has been observed. In the plot shown, this cross-talk has been removed. There are no indications of cross-talk stemming from the MAPMT itself. The common mode-noise has been subtracted. A few dead pixels also arising from the electronics chain can be seen. The loss of signal below the 5 σ threshold cut is still under study but is expected to similar to the value measured with the LED data. A quantitative analysis where, in the data, the observed yield of photo electrons is properly corrected for all these effects gives the following preliminary results: A total of 7.3 photo electrons are measured per event while 6.9 photo electrons are expected from a simulation. For similar runs without quartz lenses in front of the tubes 5.2 photo electrons were observed whereas the simulation predicts 4.6 photo electrons. The gain in detected photons by employing the lenses is 45 %. In summary, the observed number of photo electrons is about 1.1 times the expected

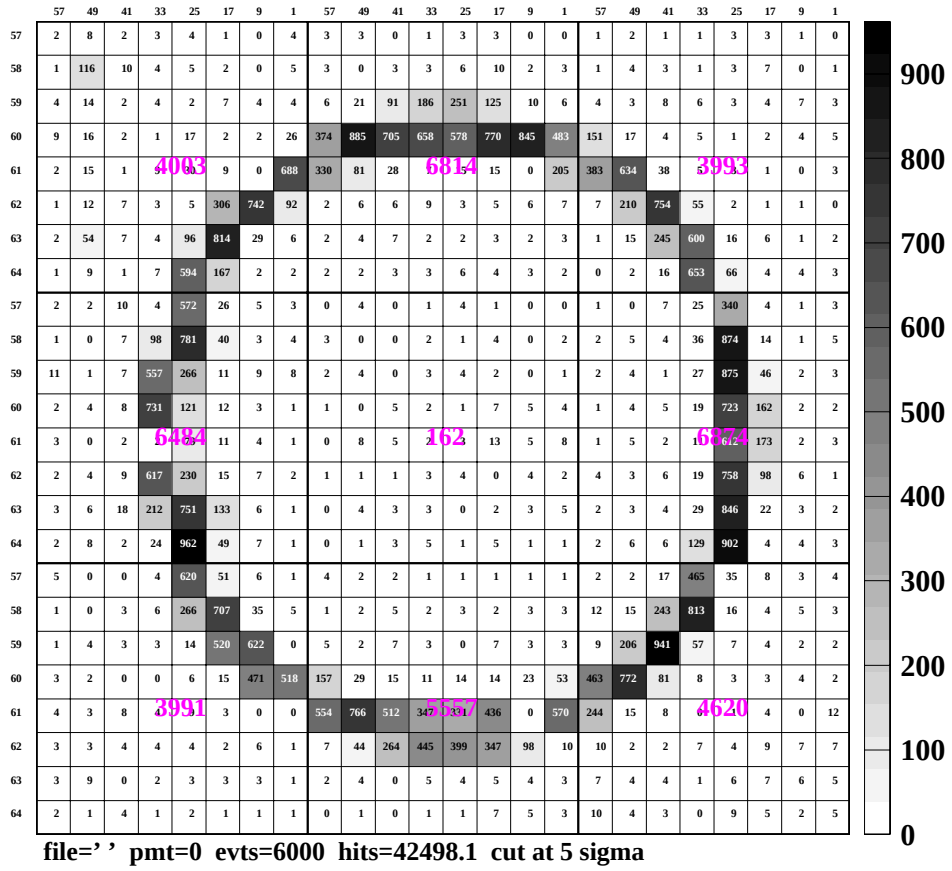

Figure 11: Cherenkov ring measured with MAPMTs using a CF_4 gas radiator at a pressure of 700 mbar with (right plot) and without (left plot) quartz lenses mounted in front of the tubes. The common-mode noise has been subtracted. Cross-talk due to the electronics chain has been corrected for.

value. The error on this ratio is still under study but should be around 10 %. An additional result is that the measured quantum efficiency varies by about ± 10% for the different tubes.

3.4 Charged Particles Traversing the Photo Detector

A few million events were also recorded during two weeks of test beam where charged particles were traversing a MAPMT. Using the CAMAC read-out, data were taken with and without a lens placed in front of the MAPMT and for different angles of the incoming particle direction with respect to the tube axis. The analysis of these runs shows that many photons produced in the quartz lens undergo total internal reflection. For most angles only between 5 to 10 photons are observed in a MAPMT

when a charged particle traverses through it. When the particles enter the quartz lens at angles of around 45 degrees signals are produced in up to 30 out of the 64 channels of a MAPMT. Given the orientation of the photo detectors in RICH 1 and RICH 2, a relatively small fraction of the charged particle flux will actually traverse through the tube under these worst case angles. The results are in a agreement with a simulation.

3.5 Magnetic Field Measurements

A MAPMT has been placed into a Helmholtz coil. Using a LED light source, we then measured its efficiency at magnetic fields of 0 to 30 Gauss. The following results have been obtained:

- The unshielded MAPMT is almost insensitive to transverse magnetic fields of 30 Gauss.
- If a longitudinal field of 30 Gauss is applied to the unshielded MAPMT the outermost rows of channels lose a sizable fraction of photoelectrons.
- If a longitudinal field of 30 Gauss is applied and the MAPMT is shielded with a 0.9 mm thick square mu-metal tube the efficiency improves considerably. The remaining loss decreases when the shielding coverage along the axis normal to the photocathode plane is increased.

The field map calculations predict field strengths of maximum $B_y = 30$ Gauss and less than 10 Gauss for the other two directions for RICH 1 and less for RICH 2 if a the a collective shield is put around the photo detector frames. Using the saturation value of about 7500 Gauss for mu-metal, we estimate that a similar shielding effect will be obtained if 0.4 mm thick mu-metal were to be used.

4 Multianode Photo Multiplier Tube Proposal

We propose to use Multianode Photo Multiplier Tubes as the photosensitive device for the Ring Imaging Cherenkov detector in the LHCb experiment. The detector technology and the principle characteristics of the MAPMT are described in Section 2. The results of the R&D program with the MAPMT are described in Section 3. Here we describe a baseline design of the LHCb RICH detector with MAPMTs as photo detectors.

4.1 Proposed MAPMT Implementation

The basic unit, called a module, consists of an array of 4x4 MAPMTs. A single quartz lens will be placed in front of each tube, separated from the UV-glass window by a small air gap. The 16 tubes are mounted onto a motherboard which distributes

the high voltage to the photocathode and the dynodes of each tube and connects the 1024 anode channels of a unit to the front-end electronics which are mounted on the back of the motherboard. In addition, the motherboard provides mechanical stability for the unit. The lateral dimensions of a tube are 25.7 $\pm$ 0.5 mm. The pitch of the tubes is 26.7 mm where the additional space is needed for shielding the tubes from the magnetic stray fields. This will be achieved with placing a grid of mu-metal sheets with thickness 0.5 mm around and between the tubes of a module. Individual quartz lenses will be mounted into this mu-metal grid. The radius-of-curvature R of the lenses has been optimised by a Monte Carlo study to be 20 mm.

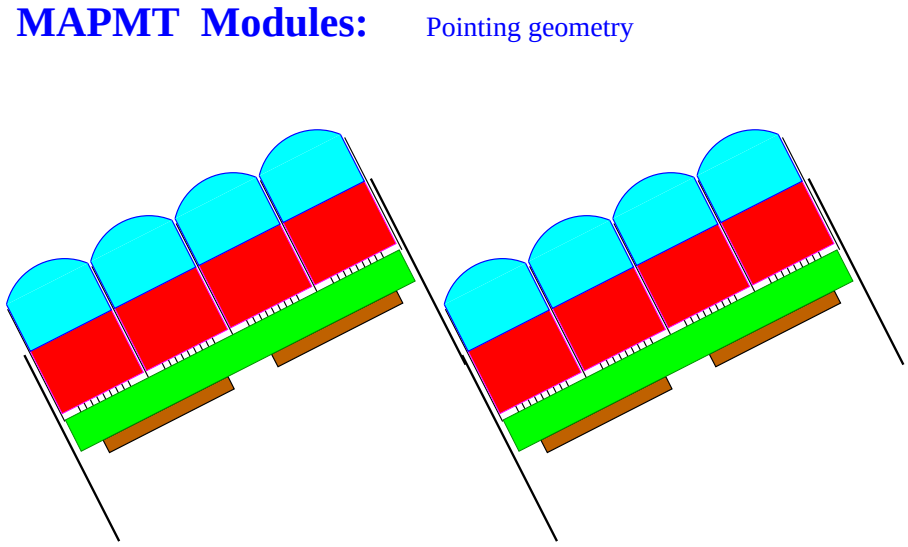

Figure 12: Schematics of pointing module (side view). Shown are MAPMTs (red), lenses(blue), the motherboard (green) with the hybrid (brown), the magnetic shields (black) and a mounting frame (black).

In the horizontal plane, the RICH mirrors will be tilted in order to allow positioning of the photo detector planes outside the acceptance of the LHCb experiment. Thus the photons will hit the photo detector planes, on average, at angles of 440 mrad and 240 mrad in RICH 1 and RICH 2, respectively. When using single lenses for each MAPMT this produces partial shadowing of the pixels at one side of the tube if the tubes are mounted parallel to the photo detector plane. We propose to tilt the modules accordingly to restore normal incidence for the mean angle of the incoming photons. Figure 12 depicts a side-view sketch of two tilted modules, separated by 2.5 mm, in RICH 1. The size of the photo detector sensitive areas (half-plane) are 600 mm x 1000 mm^2 for a RICH 1 and 640 mm x 1200 mm for a RICH 2, respectively. Figure 13 illustrates how, in the baseline design, this area is covered by 50 modules in RICH 1 and 66 modules in RICH 2, respectively. Note that some of the outermost modules only have to be partially equipped with tubes. The values of the main geometrical parameters are summarized in Table 2. A spreadsheet containing detailed information about the geometry is given in Appendix A.

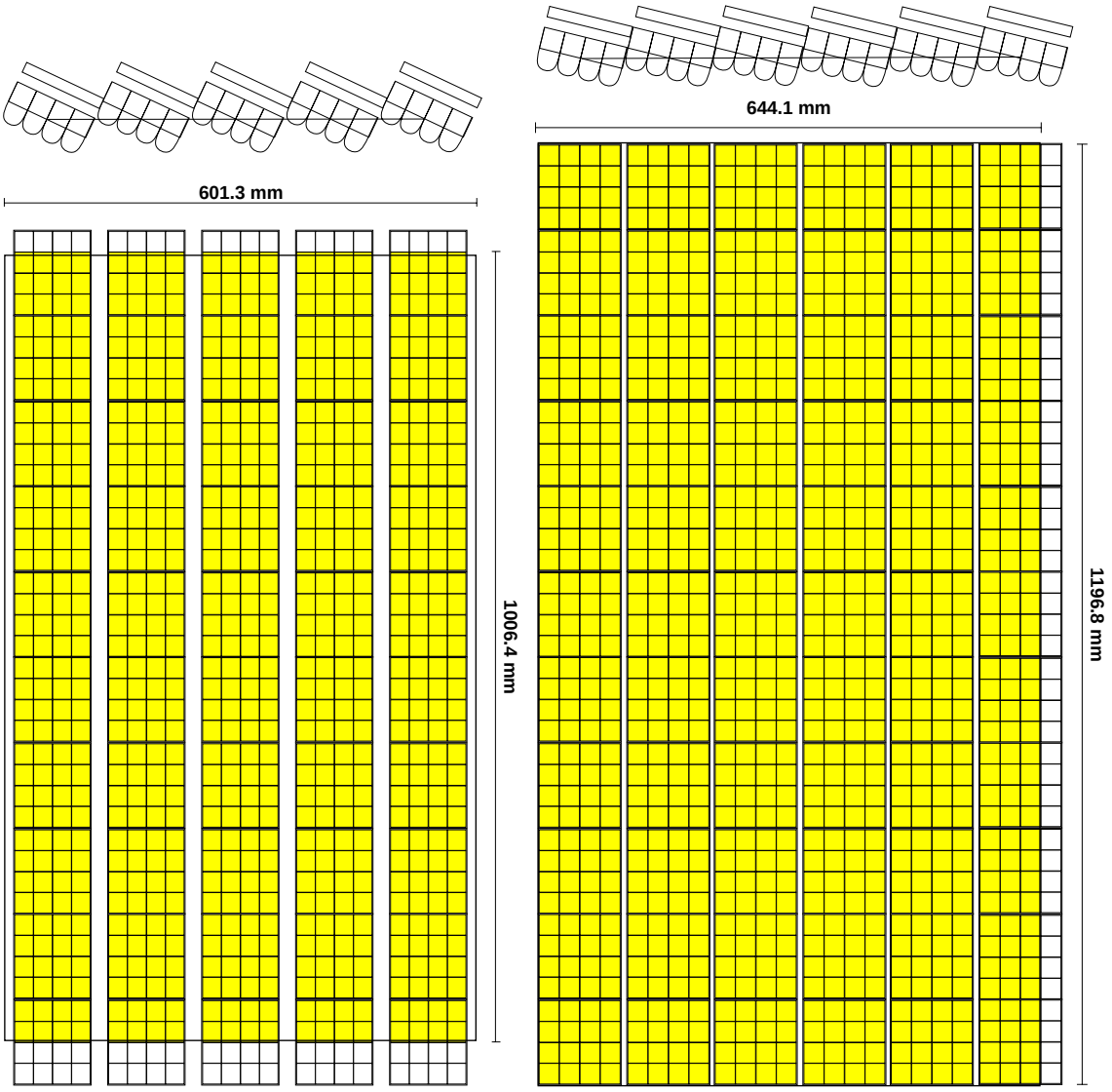

Figure 13: RICH 1 and RICH 2 half planes (front view). The MAPMTs needed to cover the photo detector sensitive area are shaded. Note that the vertical gaps between the rows will collapse to zero width if the half planes are viewed from the mean incoming photon direction.

MAPMT Modules:		
Channel pitch [mm]	2.3	
Channel active area [mm^2]	2.1 x 2.1	
Pixel size at lens [mm^2]	3.0 x 3.0	
Lens radius of curvature [mm]	20	
MAPMT pitch [mm]	26.7	
Module size [mm^2]	108.8 x 108.8	
Active/total area (filling factor)	0.79	
Half planes:	RICH 1	RICH 2
Tilt angle of modules [mrad]	440	240
Number of modules per row	5	6
Number of modules per column	10	11
Totals:	RICH 1	RICH 2
Number of modules	100	132
Number of tubes	1480	2024
RICH totals:		
Number of modules	232	
Number of tubes	3504	
Number of channels	224256	

Table 2: MAPMT Geometry.

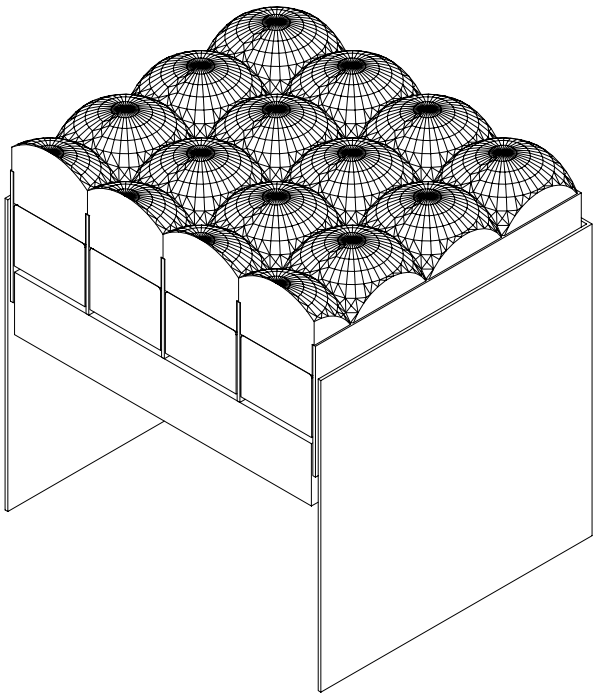

Figure 14: Engineering drawing of a 4 × 4 MAPMT module.

Detailed mechanical design studies of the photo detector mounts are underway. In Figure 14 an engineering drawing of a mechanical module including the lenses is shown. Possible improvements are that the light loss due to the air gap may be reduced by optically coupling the lens to the UV-glass window with optical grease. Spare tubes will be mounted onto the unoccupied slots of the outermost modules.

4.2 Proposed MAPMT Electronics

In this section, the front-end electronics for the MAPMT is described. One front-end chip is reading out 128 channels, therefore 8 chips are needed to read out the 1024 channels of one module. The chip is incorporated into a hybrid and mounted onto the motherboard, as sketched in Figure 12. A total of 1856 chips are needed to read-out the 232 MAPMT modules. Table 3 shows various parameters of the detector signals and the front-end chip.

At the time of the photo detector choice the baseline design foresaw analogue electronics based upon the the SCT 128A chip. While this is still the case it will become clear throughout this section, that there are a few scenarios which would change this baseline. With the MAPMT being the backup solution there is no manpower and money is available to solve the outstanding issues concerning the MAPMT for the SCT 128A chip. The choice of the front-end chip is connected to the solution which will be chosen for the vertex detector. This most likely means that if the BEETLE chip will become available, it will be selected for the vertex detector. In this case there would be advantages to also use the BEETLE chip for the MAPMT, if the change is compatible with the photo detector project schedule (see Section 4.4). The other differences to the baseline design should have no (or only favourable) consequences for other aspects of the program.

The MAPMT has a gain of 3×10^5 and the SCT 128A chip is designed to amplify a charge of 26000 e from silicon detectors. Hence the detector signals have to be attenuated. There are three possible solutions: The first one is an attenuator network, which is integrated into the hybrid and could be either passive - similar to the one used with the APVm chip for the test results in 1999 - or have active components (chip). Secondly the preamplifier stage of the front-end chip could be modified to cope with larger signals which need less amplification. This solution is chip specific, i.e. the low gain option should be included into the chip. For the SCT A128 the design will most likely not start as long as the MAPMT is a backup solution. For the BEETLE chip a few test structures have been added to the current submission. The third solution is running the MAPMT at a lower gain. This is currently under study. Preliminary results, which can be find elsewhere [9], look promising but more tests are needed.

An attenuation factor of about ten — or running the tube with a gain of only 30000 — is needed to match the dynamic range of the SCTA 128A or the BEETLE chip. We want to measure the ADC spectrum of the MAPMT from the pedestal to the upper end of the second photon. Since the single photon spectrum has a width which is of the same order of magnitude as its mean, this gives a required dynamic

range of 3 photons. To accommodate the gain variations within tubes and between tubes of a module an additional factor of 3 is needed for the total dynamic range of 9 photons. To match this large dynamic range a non-linear gain will be studied during the modification of a front-end chip.

An average signal position over pedestal width of 40 for single photons can be achieved exploiting the fact that the noise of the front-end chip will be at or below 750 e. Running at somewhat higher gain could increase this ratio which in turn would reduce the inefficiency of the tube due to the loss of signal below a threshold cut. The aim is to obtain an inefficiency of 10% or less. An average signal position over noise of 40 that has been measured during tests running the tubes at very high gains and a total inefficiency of 11.5% has been measured (see Section 3.1).

The current baseline (HPD) has a binary front-end solution (pixel chip). This impacts strongly on the development of the off-detector electronics (ODE). The feasibility of binary electronics for the MAPMT must be studied and a conclusion has to be reached before the final decision on the photo detectors. Again the BEETLE chip is planning along this route. The advantages of operating the MAPMT with binary electronics are: a) The cost effective use of optical fibre links from the detector to the ODE as proposed for the HPDs, b) ODE electronics in the counting room facilitates access and commissioning and c) no additional design work needed.

MAPMT Electronics:

Detector signals:

Rise/fall time [ns]	6
Baseline width [ns]	8
Single photon signal [e]	3.00E+05
Variation within tube	2
Variation tube to tube	2
Total variation from tubes	3
Single photon signal minimum [e]	1.73E+05
Single photon signal maximum [e]	5.20E+05
Required dynamic range [photons]	3
Total range [photons]	9
Total dynamic range lower end [e]	7500
Total dynamic range upper end [e]	1.56E+06

Front-end chip SCT 128A, Level 0:

Number of readout modules	232
Number of channels per module	1024
Number of channels per chip	128
Number of readout channels	237568
Number of active channels	224256

Number of chips per module	8
Number of chips	1856
Required shaping time [ns]	< 25
Noise [e]	750
Dynamic range lower end, ADC bit resolution [e]	500
Dynamic range upper end [e]	1.56E+05
Dynamic range [ADC bits]	8.28
Attenuator network	
Attenuation	10
Attenuated single photon signal [e]	30000
Attenuated single photon signal [ADC counts above pede	60
Signal over Noise for single photon	40.00
Signal over Noise for single photon minimum	23.09
Signal over Noise for single photon maximum	69.28
Output multiplexing rate [MHz]	40
Output multiplexing factor	32
Pipeline length [ns]	4000
Pipeline length [cycles]	160
Derandomizer depth	16
Links, Level 1:	
Number of data links per chip	4
Total number of data links	7424
Dynamic range [ADC bits]	9
Level 1 output rate [kHz]	40
Bandwith for output data without zero suppression [Gbi	85.5
Occupancy	0.03
Bits for addressing	18
Bandwith for output data with zero suppression [Gbits/	7.7
Output bandwith per multiplexer [Gbits/s]	4
Number of multiplexers with zero suppression	2
Channels per VME board	96
How many VME modules	78

Table 3: MAPMT Electronics.

4.3 Performance

In this Section the results of the performance studies will be summarized. The full results can be found elsewhere [10]. A full simulation using the parameters of the

baseline design if possible gives the following preliminary results (Table 4):

	Aerogel	C_4F_{10}	CF_4
Number of detected photo electrons	8.7	29.7	15.3
Cherenkov angle resolution [mrad]	1.91	1.45	0.46

Table 4: Number of photo electrons for $\beta = 1$ tracks and Cherenkov angle resolutions for the 3 different radiators.

Figure 15 shows the matrix of assigned hypothesis vs true particle type when backgrounds as well as charged particles are included in the simulation. The corresponding efficiencies for pion and kaon identification are 87 % and 89 %, respectively. The rate of misidentifying a pion as a kaon or a proton is 1.1 % and the rate of misidentifying a kaon as a lighter particle is 2.7 %, respectively. Table 5 gives the

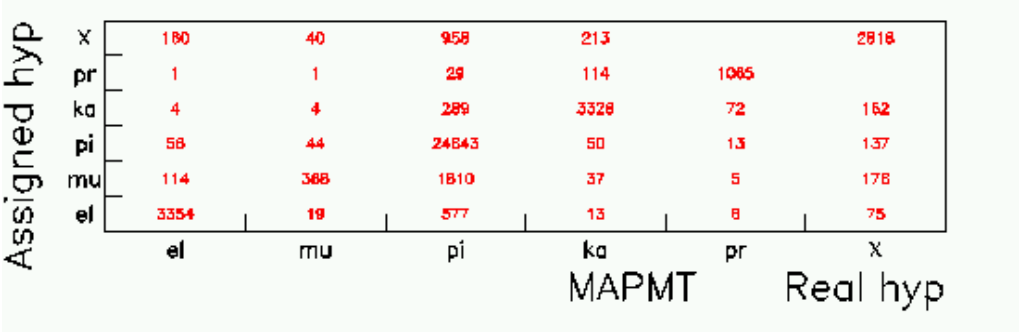

Figure 15: Results from the pattern recognition for the assigned hypothesis versus the true particle type. Each track gives one entry in the table. The track types (1,2,3,4,5,6) correspond to (e, μ, π, K, p, X) where X denotes tracks below threshold in all radiators.

efficiencies and purities for the benchmark channels $B_d^0 \to \pi^+\pi^-$ and $B_s^0 \to K^+K^-$. The kaon tagging efficiency and mistag rate are 31 % and 32 %, respectively.

	Efficiency	Purity
$B_d^0 \to \pi^+\pi^-$	0.906	0.813
$B_s^0 \to K^+K^-$	0.881	0.877

Table 5: Efficiencies and purities for the MAPMT for two benchmark channels.

4.4 Schedule

A schedule for the baseline design of the MAPMT RICH project made at the time of the photo detector choice is shown in Table 6. At the end of 1999 the MAPMT has been selected as backup choice for the photo detectors. This decision clearly has

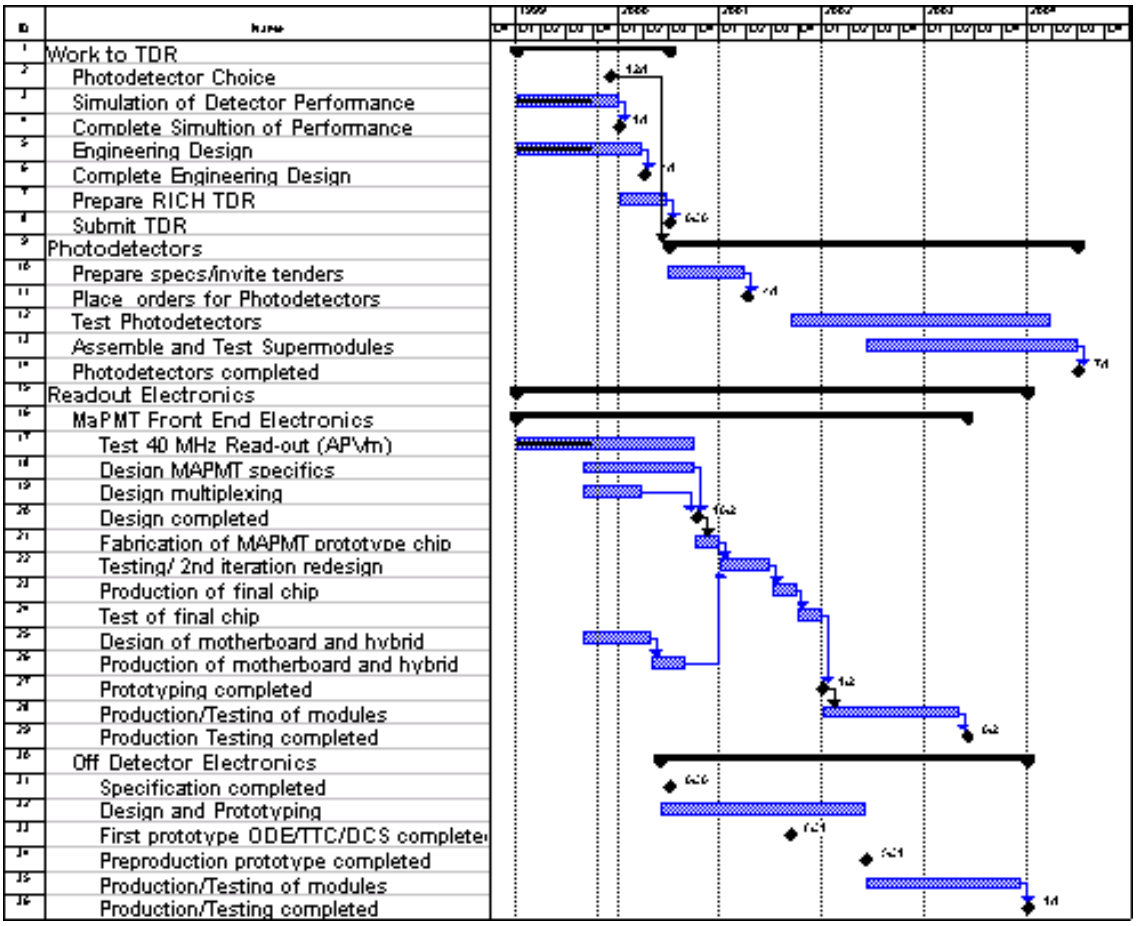

Table 6: Obsolete RICH MAPMT project schedule up to July 2004 made at the time of the photo detector choice (11/1999).

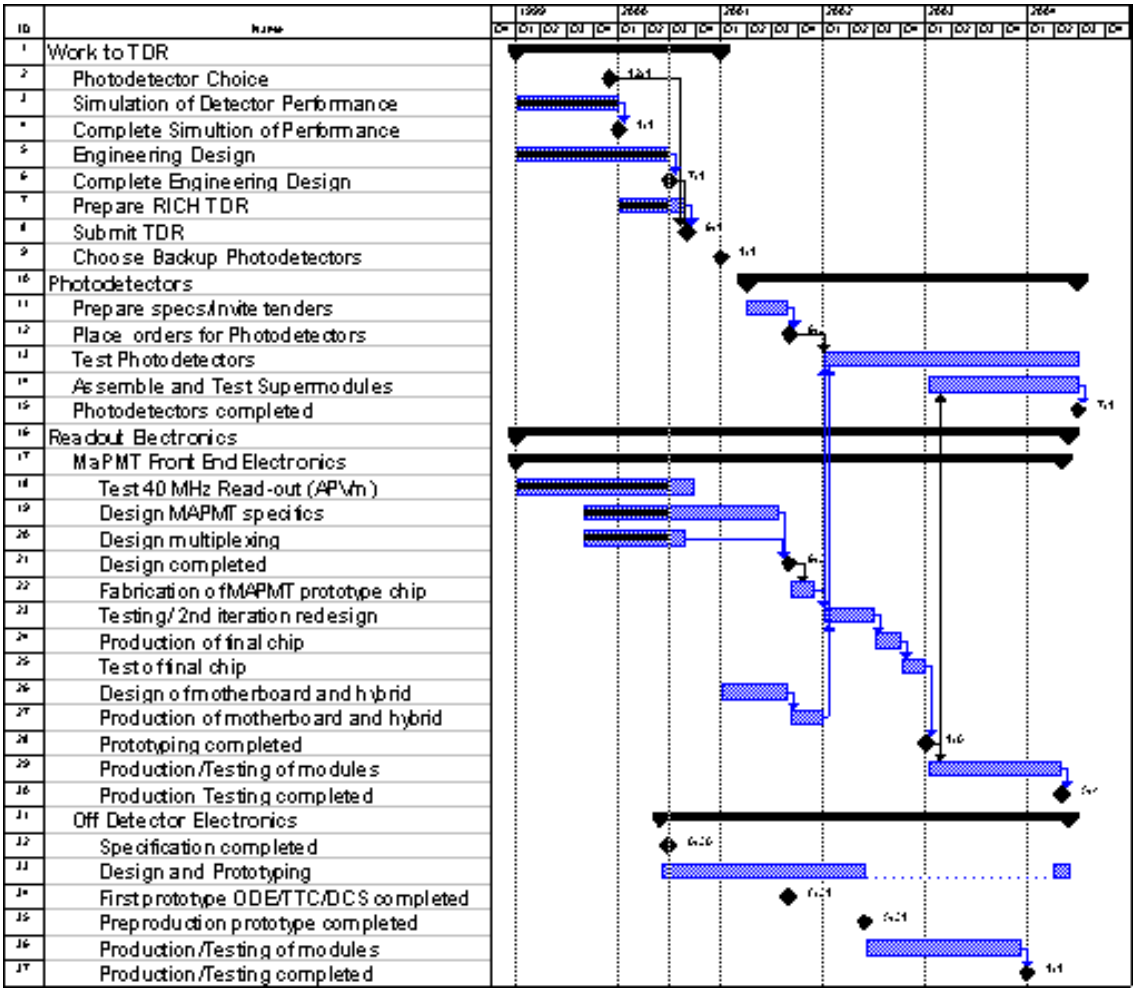

Table 7: Updated RICH MAPMT project schedule up to July 2004 when we will start to assemble the RICH detectors at CERN.

implications for this project schedule. We present an updated schedule in Table 7. Regarding the photo detector schedule we can see that the ordering of the MAPMTs has been delayed by 6 months to 9/2001. This delay still allows us to be ready to start assemble the RICH detectors at CERN in July 2004. The testing of the tubes will start around 2/2002. Delivery of the tubes will take about 2 years. Testing of the tubes again takes about 2 years, assuming that 2 photo detector testing facilities will be built and that modules can be tested at a rate of 1 to 2 per week.

The changes to the schedule of the front-end electronics for the baseline solution are as follows: The design of the MAPMT gain adaption to a silicon chip is delayed by one year and will be completed by 9/2001. This delay shifts all subsequent tasks by the same amount. The design and production of the motherboard and hybrid will not start before we decide to go with the backup solution and has been delayed by 1 year 3 months and will not be available before 1/2002. The physicists/electrical engineers who are interested in this project are currently working on the corresponding task for the pixel HPD. If a second iteration for the front-end chip becomes necessary the prototyping of the front-end electronics will be finished only by 1/2003.

The front-end chip and the motherboard/hybrid are now the most time critical parts of the project. A few working motherboards and hybrids plus front-end chips are needed before we can start the testing of large quantities of MAPMTs. Of these the motherboard/hybrid is very serious since there is hardly any possibility of saving time. The schedule of the front-end chip would be shortened if the MAPMT could be operated at lower gains without the need of a redesign or attenuator network (see Reference [9]). The test of a RICH half-plane or a large fraction of it in the 2003 test beams at CERN is also very critical since the production and testing of the final modules will not start before 1/2003. The ODE schedule would benefit if the MAPMT were operated with binary electronics since there would be no need of additional design and development compared to the baseline option.

4.5 Costs & Manpower

In the TP, MAPMTs were considered primarily as a backup solution due to their prohibitive price. Since then, Hamamatsu has made a price offer comparable to the HPD's, thus making the MAPMT a contender for the photo detector technology. Below preliminary cost estimates are presented.

Since industry would supply the photo detectors, no manpower is required for production of the MAPMTs. The staff-years for testing the photo detectors and designing and testing the front-end as well as the back-end electronics is available at the participating institutes.

MAPMT Costs (preliminary):

Costs

MAPMT and Level 0:

	Number of units	Unit cos[kSFr]	Cost [kSFr]
MAPMT tubes	3504	0.931	3262.2
Lenses	3504	0.070	245.3
SCT 128 A chip	1856	0.130	241.3
Hybrid	1856	0.070	129.9
Motherboard	232	2.000	464.0
TTCrx+DCs	232	0.100	23.2
Data links, Level 0	7424	0.009	69.6
Total MAPMT and Level 0			4435.5
Level 1:			
Trigger/clock links	464	0.180	83.5
9U VME Level 1 boards	78	5.000	390.0
VME crates	5	10.000	50.0
Multiplexer units	2	2.500	5.0
Read-out unit Level 1 to DAQ	2	5.000	10.0
Total Level 1			538.5
Total Cost			4974.1

Table 8: MAPMT Costs.

5 Summary

We have presented a proposal to use multianode photomultiplier tubes as photosensitive devices for the LHCb RICH detector. The characteristics of the MAPMT, results from R & D studies and their expected performance in a baseline design for the LHCb RICH have been presented. The baseline design has been described in detail which include time schedules and cost estimates.

References

[1] "A Large Hadron Collider Beauty Experiment for Precision Measurements of CP Violation and Rare Decays"; LHCb Technical Proposal, LHCC 98/04, LHCC/P4 (Feb. 1998).

[2] The LHCb RICH detector web page: "http://lhcb.cern.ch/rich/".

[3] R. Forty, "Use of lenses to increase the RICH photodetector coverage", LHCb/98/038.

[4] V. Gibson *et al.*, "Performance of a Multianode Photo Multiplier Cluster equipped with Lenses", LHCb 2000-083 RICH.

[5] A. Duane *et al.*, "Cherenkov Rings Detected with a Multianode P.M.T.", LHCb/98/039 RICH.

[6] N. Smale *et al.*, "Evaluation of the Multianode Photomultiplier for the LHCb RICH detectors", LHCb/98/066 RICH.

[7] E. Albrecht *et al.*, "Latest beam test results from RICH prototypes using hybrid photo detectors and multi anode PMTs", Nucl. Inst. Meth. **A 433** (1999) 159.

[8] E. Albrecht *et al.*, "A Prototype RICH Detector Using Multi-Anode Photo Multiplier Tubes and Hybrid Photo-Diodes", LHCb 2000-068 RICH, submitted to Nucl. Inst. Meth. **A**.

[9] S. Eisenhardt *et al.*, "Study of Multianode Photo Multiplier Tubes at Low Gains", LHCb 2000-088 RICH.

[10] R. Forty, G. Wilkinson, "A simulation study of the LHCb RICH performance", LHCb 2000-066 RICH.

A MAPMT Geometry

Specification of MAPMT Photo Detectors
for LHCb RICH

Geometry

Single Multianode Photo Multiplier Tube (MAPMT)

Number of channels	64
Number of channels per row	8
Number of channels per column	8
Total size [mm^2]	26.2x26.2
Channel pitch [mm]	2.3
Channel active area [mm^2]	2.1x2.1
Channel dead region [mm]	0.2
Total active size [mm^2]	18.2x18.2
Lens active size [mm^2]	26.2x26.2
Pixel size at lens [mm^2]	3.023x3.023
Demagnification factor	1.440
1/(demagnification factor)	0.695

Module

Number or MAPMTs	16
Number or MAPMTs per row	4
Number or MAPMTs per column	4
Total number of channels	1024
MAPMT pitch [mm]	26.7
Space between MAPMTs [mm]	0.5
Total active size [mm^2]	104.8x104.8
Frame width [mm]	1.25
Total size [mm^2]	108.8x108.8
Active/total area (filling factor)	0.791

Half Plane RICH 1

Number of horizontal modules	5
Number of vertical modules	9.25
Total number of modules	50
Total number of tubes	740

Total width [mm]	544.0
Total height [mm]	1006.4
Tilt angle [rad]	0.440
Effective module width [mm]	120.3
Effective total width [mm]	601.3

Half Plane RICH 2

Number of horizontal modules	5.75
Number of vertical modules	11
Total number of modules	66
Total number of tubes	1012
Total width [mm]	625.6
Total height [mm]	1196.8
Tilt angle [rad]	0.240
Effective module width [mm]	112.0
Effective total width [mm]	644.1

RICH 1

Number of half planes	2
Total number of modules	100
Total number of MAPMTs	1480
Total number of channels	94720

RICH 2

Number of half planes	2
Total number of modules	132
Total number of MAPMTs	2024
Total number of channels	135168

RICH Totals

Total number of modules	232
Total number of MAPMTs	3504
Total number of channels	224256